5. Electrochemical Study of Tin/Tin Oxides Interface

5. Electrochemical study of tin/tin oxides interface

In this chapter, the electrochemical study of tin is explained. The main aim of this study has been to acquire a precise knowledge of the electrochemical oxidation of metallic tin, that has been performed as the first stage of the electrochemical study of gas sensors based on tin(IV) oxide. As the gas-sensing mechanism is based on the fact that the oxidising/reducing agents (i.e., gases) exchange charge with the SnO_2 material, thereby changing its electrical properties by means of electrochemical reactions, the current models for charge exchange at this interface that, at the present stage, have been built from indirect or non-rigorously controlled experiments, should be tested in rigorous electrochemical experiments.

Thereby, the chapter begins with a brief introduction where the main features of semiconductor electrochemistry are explained. This section has not the aim to be systematic, and the reader interested in a more detailed discussion is referred to the bibliography [127-134]. Afterwards, the obtained results are presented and discussed.

5.1. Introduction

The study of semiconductor electrodes began with the works of W. H. Brattain and C. G. B. Garrett in the mid-50's, and it has greatly influenced the concepts of electrochemistry. The electrochemistry of semiconductors is a vast multidisciplinary field that studies phenomena of great interest for both solid-state physicists and metal electrochemists, and the main difference with respect to "classical" electrochemistry (i.e., that of metals) is that in a semiconductor, electrochemical reactions depend not only on the applied potential but also on the availability of the corresponding free carriers. Thus, for example, in the dark, no hydrogen evolution occurs on a p-type semiconducting electrode, while no oxidation is observed on an n-type electrode because of the absence of free carriers in both cases. Light can be employed to generate the necessary charge carriers in each case (electrons in p-type semiconductors, holes in n-type).

5.1.1. Description of electron behaviour in semiconductors

In general, the density of energy states of electrons in a solid can be obtained by solving Schrödinger's equation. Thus, it is observed that, in one covalent atom, electronic states are discrete, but when the orbitals of many atoms overlap to form a solid, their discrete energy states form energy bands. In the case of a semiconductor, the electronic states do not form a continuum of states, as in the case of metals, but form two different energy bands: the conduction band (CB) at energies $E>E_C$ and the valence band (VB) at energies $E<E_V$ (fig. 5.1.). The two different bands are separated by the forbidden band gap $E_g = E_C - E_V$, that is a gap of energies where no charge carrier can be placed because there are no available electronic states.

The energy of electrons in solids is expressed in eV with respect to the vacuum level $E_{vac} = 0$ (energy of electrons at rest in vacuum), that is called the absolute energy scale. The electronic affinity (E_A) and the ionisation energy (E_I) are usually given in this scale. At T = 0 K, the VB is completely filled, and the CB is empty, so the material is insulating. At T > 0 K, some electrons will be thermally excited to the CB, giving the material a certain electrical conductivity (note that this process can also be promoted by photons of energy $h\nu \geq E_g$). When an electron is excited to the CB, the vacancy left in the

VB is an empty valence state of one atom that can easily be occupied by a valence electron of a neighbouring atom. Of course, this will result in the creation of an empty valence state in the neighbouring atom, and the process can be repeated several times. For convenience, this phenomenon is described as a hole that travels in the opposite direction, rather than as valence electrons successively occupying the vacancies that the others have left behind. Holes are then regarded as positive free charges having an energy in the VB, and also contribute to the conductivity.

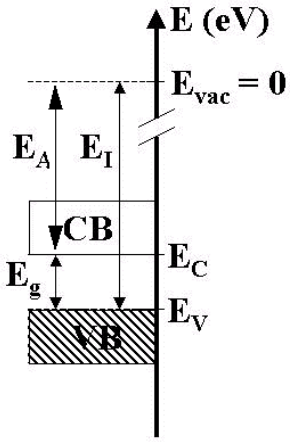

Fig. 5.1. *Electronic energy states in a semiconductor.*

The probability of a state energy E to be filled by an electron is given by the Fermi-Dirac statistics:

$$f(E) = \frac{1}{1 + e^{\frac{E - E_F}{k_B T}}}$$

where $k_B = 8.6 \bullet 10^{-5}$ eV/K is the Boltzmann constant and E_F is the Fermi energy level. As explained above, at 0 K all states of energy lower than E_F are filled with electrons (f(E)=1) and the states of higher energy are empty (f(E)=0) and, as the temperature increases, a distribution is formed around E_F, for which the occupancy is always $f(E_F)=1/2$. In many cases, the electron and hole concentrations (n and p respectively) are small. The Fermi energy is then located within the gap, and at a distance from the bands of at least a few times k_BT. In such conditions, it can be approximated by a Maxwell-Boltzmann distribution.

$$f(E) = e^{-\frac{E - E_F}{k_B T}}$$

The concentration of charge carriers (electrons in the CB and holes in the VB) is then:

$$n = N(E_C) \cdot f(E_C) = N_C \cdot e^{-\frac{E_C - E_F}{k_B T}}$$

$$p = N(E_V) \cdot (1 - f(E_V)) = N_V \cdot e^{-\frac{E_F - E_V}{k_B T}}$$

where N_C, N_V are the effective state densities at the bottom of the CB and at the top of the VB respectively. As in semiconductor solids conduction occurs by movement of electrons in the CB or holes in the VB, the electric conductivity depends on the electron and hole concentrations.

The conductivity can be increased by adding atomic impurities in the semiconductor. The semiconductor is then called extrinsic or doped. These external atoms generally introduce additional electronic energy states in the gap, being of most interest the so-called "shallow" impurities. Shallow-donor impurities, such as P in Si, introduce states at energy levels E_D located close to the CB. In the case of stoichiometric SnO_2, no shallow-donor impurities will be present. Nevertheless, the presence of oxygen vacancies in SnO_2 are usually detected. These vacancies can be understood as Sn(II) species in the crystal, i.e., Sn atoms not fully oxidised to Sn(IV). Thereby, they can alternate between II-IV exchanging two electrons with the neighbouring Sn(IV), which then become Sn(II), thus resulting in the electron travelling throughout the material. This can be described using the band theory as electrons of doping species that are delivered to the CB of the whole crystal, thereby behaving as free carriers.

These states are filled at low temperature but, since $E_C - E_D$ is small, these states soon become ionised as the temperature is raised, and the "donated" electron move into the CB. In this case, the concentration of conduction electrons is approximately equal to the concentration of donor impurities N_D ($n \approx N_D$), and the semiconductor is referred to as "n-type". Since n>>p, electrons in n-type semiconductors are called majority charge carriers. The Fermi energy is given by

$$E_F = E_C - k_B T \cdot \ln \frac{N_C}{N_D}$$

and it is located close to the CB. The energy difference between the Fermi level and the majority carrier band is:

$$\mu_C \equiv E_C - E_F^n = k_B T \cdot \ln \frac{N_C}{N_D}$$

A similar discussion is valid for p-type semiconductors with electron-accepting impurities (acceptors), as B in Si.

5.1.2. Semiconductor behaviour in presence of an electrolyte

When the semiconductor is immersed into an electrolyte, the Fermi energy of them, i.e., the electrochemical potential of the electron in both phases (that, in general, are different) equal because electrons flow from the phase of higher E_F towards the lower. This process produces the separation of charges of opposite sign, giving rise to an arrangement of charged layers at both sides of the interface. As the treatment of potential distribution in the electrolyte can be found elsewhere, here we will only give a brief description of the capacitance and potential distribution that arises in the semiconductor due to this process.

Thus, if the Fermi energy of the semiconductor is located within the bandgap, the equalisation of the Fermi levels with the electrolyte is achieved by the transfer of majority carriers to the latter. At equilibrium, the semiconductor surface is thus depleted of majority carriers, and the "charge layer" (named space charge region, SCR) is due to the fixed ionised dopants in the lattice. Such *depletion layer* of an n-type semiconductor is shown in fig. 5.2.b. Emptying the n-type semiconductor of electrons corresponds to a decrease in the

Fermi energy (the electrode potential shifts towards positive values). This bends the bands upward in the region contiguous to the interface. The band bending results from the internal electric field in the SCR: when the n-type semiconductor is emptied of free electrons (by electron transfer to the electrolyte, or by applying an external positive potential to the electrode) they are first depleted from the surface, which breaks the neutrality in this region and leaves a positive net charge due to the ionised donors. The fixed charge gives rise to a local electric field in the region contiguous to the surface, that attracts electrons towards the surface (i.e., opposed to the external field). The electric work delivered to an electron by the field in this region results in an increase of the electron energy near the surface, in relation to the semiconductor bulk. The upward band bending corresponds to an energy barrier for electrons. In this case, the positive charge due to the dopant ions is balanced by a negative countercharge in the electrolyte side. Note that during the formation of the depletion layer, the entire band structure in the semiconductor bulk "shifts" downward, and the bands bend so that the bandedge energy remains constant (the bandedges are "pinned" at the surface).

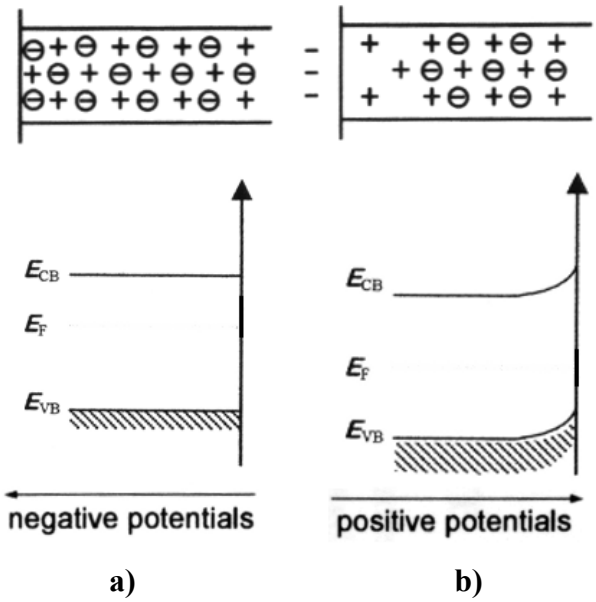

Fig. 5.2. *Energy bands profiles and charge distribution near the surface of n-type semiconductors: a) Flatband and b) Depletion. (+) are fixed charges in the crystal (eg Sn(II) atoms) that form the SCR. (-) are mobile electrons.*

The *flatband* (FB) potential, U_{FB}, corresponds to the situation in which the bands are flat, i.e. when the energy level of the bulk is the same as the one on the surface (fig. 5.2. a). There is no surface barrier and the charge due to fixed ions is balanced by the free charge at the surface. When the charge stored in surface states and due to ion adsorption can be neglected, at the FB potential the total charge at the interface is zero: $Q_{SC} = Q_{el} = 0$ at $U = U_{FB}$.

Under depletion conditions, the so-called Mott-Schottky relation can be derived:

$$C_{SC} = \sqrt{\frac{\varepsilon\varepsilon_0 e N_{SC}}{2}} \cdot \frac{1}{\sqrt{|U_S| - \frac{k_B T}{e}}}$$

From this relation, it can be deduced that the capacity of storing charge in the semiconductor depends on the material (ε) and the doping density (N_{SC}) as well as on the band bending U_S. The capacitance decreases on increasing the band bending, due to the "limited" density of dopant ions that provide the charge in the semiconductor under depletion conditions.

Thus, in general, at the equilibrium, the total charge inside the semiconductor Q_{SC} and in the electrolyte double layer Q_{el} are equal and opposite in sign. The potential drop

$$\frac{1}{C_{total}} = \frac{1}{C_{SC}} + \frac{1}{C_{el}}$$

over the interface, $\Delta\phi$, is partitioned between the semiconductor ($\Delta\phi_{SC}$) and the electrolyte ($\Delta\phi_{el}$) depending on their respective capacitances.

When the semiconductor is in *depletion*, $C_{el} >> C_{SC}$ and $C_{total} \approx C_{SC}$. The physical interpretation is that the electrolyte double layer is much thinner than the SCR because its charge density is correspondingly larger than in the depleted semiconductor. In this case, most of the potential applied to the entire interface is borne by the SCR, and is employed in the bending of the bands ($\Delta\phi_{SC}$). While the semiconductor is in depletion, the energy of the bandedges at the surface remains nearly constant ("bandedge pinning"). In contrast, inside a metal electrode no SCR is developed, and all the applied potential is dropped over the electrolyte double layer.

5.1.3. Experimental measurements

The description of the semiconductor in terms of the energy bands is valid, strictly speaking, in the bulk of the material. A surface is such a strong discontinuity that new electronic states (i.e., surface states) generally appear. In covalent crystals, the formation of a surface can be considered by breakage of the covalent bonds in a plane of a perfect monocrystal in vacuum, which give rise to half-occupied orbitals ("dangling bonds"). These surface states are named "intrinsic" (Shockley states for a covalent crystal) and their electronic energy is usually located near the centre of the bandgap. The occupancy of these states is given by a Fermi-Dirac distribution and produces a net charge on the surface. Thus, in vacuum, any surface has almost inevitably a charge located on it. Surface states are real "charge-reservoirs" that can store a charge equal to the SCR, and even larger. Electrons are exchanged between the semiconductor and the surface states, until their Fermi levels are equalised and a SCR is formed.

When a semiconductor electrode is immersed in an electrolyte, the interaction with the solvent and the chemical species in solution usually prevail, and the surface state charge may vary. The Mott-Schottky relation links the semiconductor capacitance C_{SC} under depletion, and the potential drop in the semiconductor $\Delta\phi_{SC}$. In the depletion regime, and in the absence of charge trapped at the surface ($\Delta\phi_{el} = 0$), $\Delta\phi_{SC}$ can be expressed as a

function of the electrode potential: $\Delta\phi_{SC} = U - U_{FB}$. Thus, the MS relation can be rewritten as follows:

$$\frac{1}{C_{SC}^2} = \frac{2}{\varepsilon\varepsilon_0 e N_{SC}} \cdot \left(\Delta\phi_{SC} - \frac{k_B T}{e} \right) = \frac{2}{\varepsilon\varepsilon_0 e N_{SC}} \cdot \left(U - U_{FB} - \frac{k_B T}{e} \right)$$

The capacitance C_{SC} can be measured experimentally at different electrode potentials, and the plot of $1/C^2$ vs U that is obtained is a linear relation ("Mott-Schottky (MS) plot"). Its slope yields the semiconductor doping concentration N_{SC}, and the intercept at $1/C^2=0$ allows to determine U_{FB}. It must be stressed that the capacitance that is measured experimentally is the *interface* capacitance C_{total}, including contributions of the SCR, the electrolyte double layer as well as surface states if they are present. Thus, unless an electric model for each contribution is available, the capacitance measurement must be performed under conditions such that the only significant contribution is due to the SCR: C_{el} must be large, the frequency high enough so that surface states are "frozen" and of course, low-impedance electric contacts in the circuit are essential.

5.2. Results

As has been previously discussed, the results presented below have been performed as the first stage of the rigorous electrochemical study of tin oxide gas sensors. Thus, the use of borate buffer solution allows us to have a Sn electrode under potentiostatic control in a solution able to oxidise/reduce it reversibly under the desired, highly reproducible conditions. It also allows to make measurements of the electrical (electronic) properties of the SnO_2 material sandwiched between the metallic Sn substrate and an 'ionic conductor' (i.e., the electrolyte), which is a non-destructive contact. With respect to gas sensors, the presence of an electrolyte allows to measure charge exchange processes between the SnO_2 and electroactive species dissolved in the electrolyte for this purpose, thereby allowing to investigate the response of the semiconductor to the presence of gases, but keeping the electric contact, unlike in the case where a gas phase is present, as no contact is available at the sensor surface.

5.2.1. Polycrystalline tin

As has been previously discussed, the major part of the experiments has been done in a borate solution at pH = 7.5. When polycrystalline tin is immersed in this solution, the typical voltammogram obtained is the one shown in fig. 5.3.

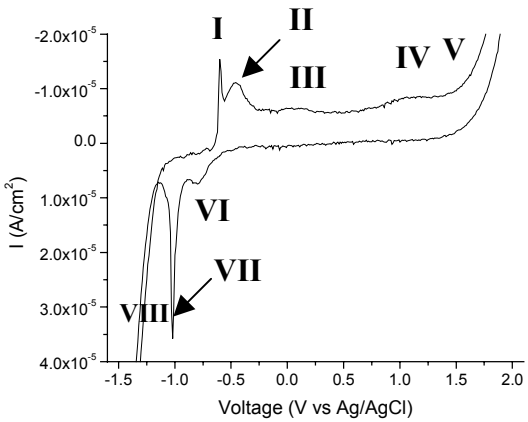

Fig. 5.3. *Second cycle of a cyclic voltammogram of tin in borate buffer at pH= 7.5. Scan rate is 5mV/s.*

This voltammogram begins at –1.6 V (remember that all potentials are referred to Ag/AgCl), where hydrogen evolution is clearly visible, and that corresponds to the metallic region. Its greatest positive potential is +2.1 V, where oxygen evolution can be also observed, being this one the highest potential used in the experiments. Thus, in this voltammogram, five oxidation peaks (from I to V) and three reduction peaks (from VI to VIII) are observed. The nomenclature of these peaks will be maintained throughout this section to identify them.

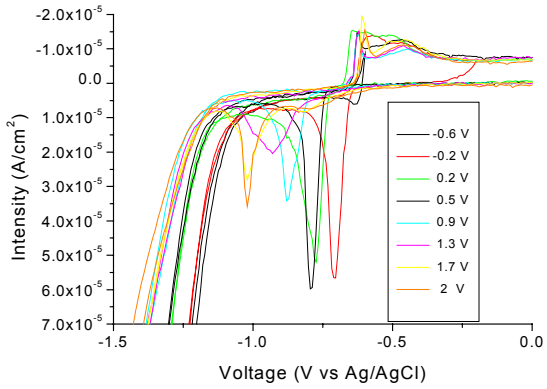

Fig. 5.4. *Second cycle of different cyclic voltammograms, varying the upper potential. Scan rate = 5mV/s.*

When a more systematic study was performed in this system, it was observed that, after applying a certain upper potential (typically greater than 0V vs Ag/AgCl approximately) to the tin electrode, it was not possible to reproduce the cyclic voltammogram at upper potentials lower than the one applied, even after 30 minutes at –1.8 V. With respect to a certain voltammogram, the first cycle features depend on the sample used, but the second cycle (and the following ones) were always reproducible when comparing fresh tin samples and samples where a certain upper potential (equal or lower than the one used for the study) was applied. Thus, in order to have well-defined departure surfaces, the procedure used for the systematic study of the behaviour of tin was as follows: previous to any experiment, 15 minutes of reduction at –1.6 V were applied to all samples in order to reduce air-born oxide, and the experiments were done beginning with the lowest positive potential and increasing this potential. Thus, it can be observed (see fig.

5.4.) that, when the upper potential of the voltammogram is changed, there is no significant change of the oxidation peaks, but there is a change of both the current of the hydrogen evolution and the position of the peak VII. Thus, at greater upper potentials the current of the hydrogen evolution is lower and the position of peak VII is shifted to more negative values. It can be also observed that peak VI is only present when the upper potential reached in the scan is high enough (of, at least, 1.3 V vs Ag/AgCl) and its position does not change when changing the upper potential. Moreover, when comparing different cycles, it can be seen that, while the areas and positions of peak VI and VII only depend on the upper potential reached, the hydrogen evolution diminishes when applying successive cycles, but the change is much lower than when comparing the change between the two first cycles.

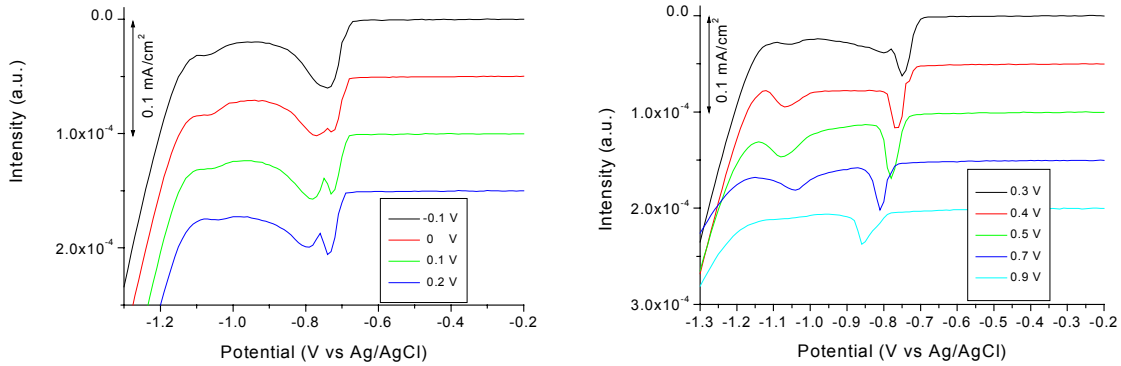

Fig. 5.5. *Scannings at 5mV/s of tin oxidised for 10 min at different potentials.*

With this behaviour in mind, a systematic study of the reduction peaks was performed in order to have a better insight of the causes that induce the observed changes. For that purpose, the following protocol was established: the samples were reduced during 15 min at –1.6 V, thereby applying by pulse the desired potential during 10 min (this time was previously determined to be long enough to avoid changes due to an incomplete oxidation), followed by a scanning (at a scan rate of 5 mV/s) beginning at the applied potential and finishing at –1.6 V. The study has been done for all the upper potentials from –0.7 to 2.1 V, each 0.1V, and the general behaviour observed is the same as that of the cyclic voltammetry. Nevertheless, there was a certain region of potentials (from 0 to 0.7 V, shown in fig. 5.5.) where an additional peak, not present in the voltammogram, was observed. This peak was, as a first guess, attributed to diffusion processes and, as it was not the aim of this work to study such processes, in order to avoid them we also investigate higher scan rates and shorter oxidation times. It must also be stated that the change of the width of the reduction peak observed after oxidation at 0.9 V vs Ag/AgCl might be due to film disordering due to the oxygen diffusion through the film necessary for the complete oxidation to SnO_2.

It can be observed that, while the voltammogram at 15 mV/s is similar to that at 5 mV/s, when applying a faster scan rate an additional reduction peak (peak IX) is detected. This peak, showed in fig. 5.6, has an area that decreases with subsequent scannings and, more interestingly, it is only observed when working with fresh tin samples, because when this peak disappears it is not observed again even after 15 minutes of reduction at –1.6 V.

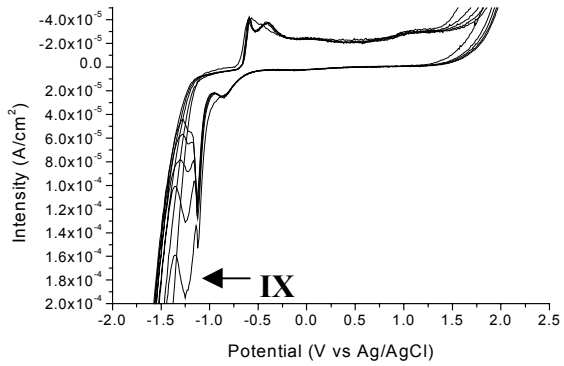

Fig. 5.6. *Cyclic voltammogram at 20 mV/s.*

Then a series of systematic experiments were performed at 15 mV/s. Some of them are showed in fig. 5.7, that also shows that the behaviour is the same as that presented at 5 mV/s.

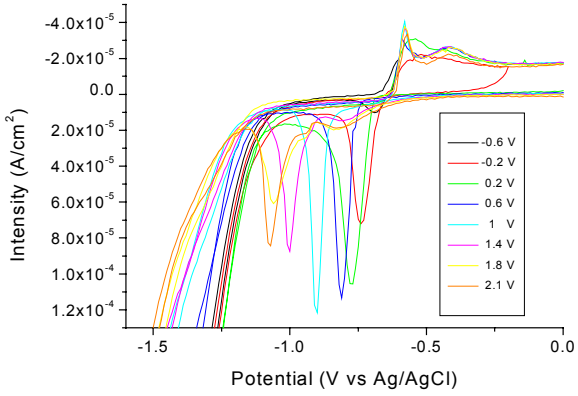

Fig. 5.7. *Cyclic voltammograms performed at 15 mV/s and different upper potentials.*

Thus, the systematic behaviour of the reduction peaks was studied using the same protocol as in the case of 5 mV/s. In order to avoid the additional peaks there observed, the oxidation times were also shortened, using either 1 minute or 10 seconds. The behaviour is similar in both cases, and is the same as that observed in the cyclic voltammograms. Nevertheless, the systematic analysis also reveals additional peaks, even with the shorter oxidation time.

As these peaks are again only observed in these experiments and not in the cyclic voltammograms, we have performed a Gaussian fit of the peak labelled as VII in all the spectra acquired with all the reduction scannings performed. It was chosen as peak VII the one more similar to that of cyclic voltammetry. Together with the Gaussian fit of the peak VII, the intensity of the reduction current at –1.59 V (where hydrogen evolution is clearly present) was also measured. The results are presented in fig. 5.8.

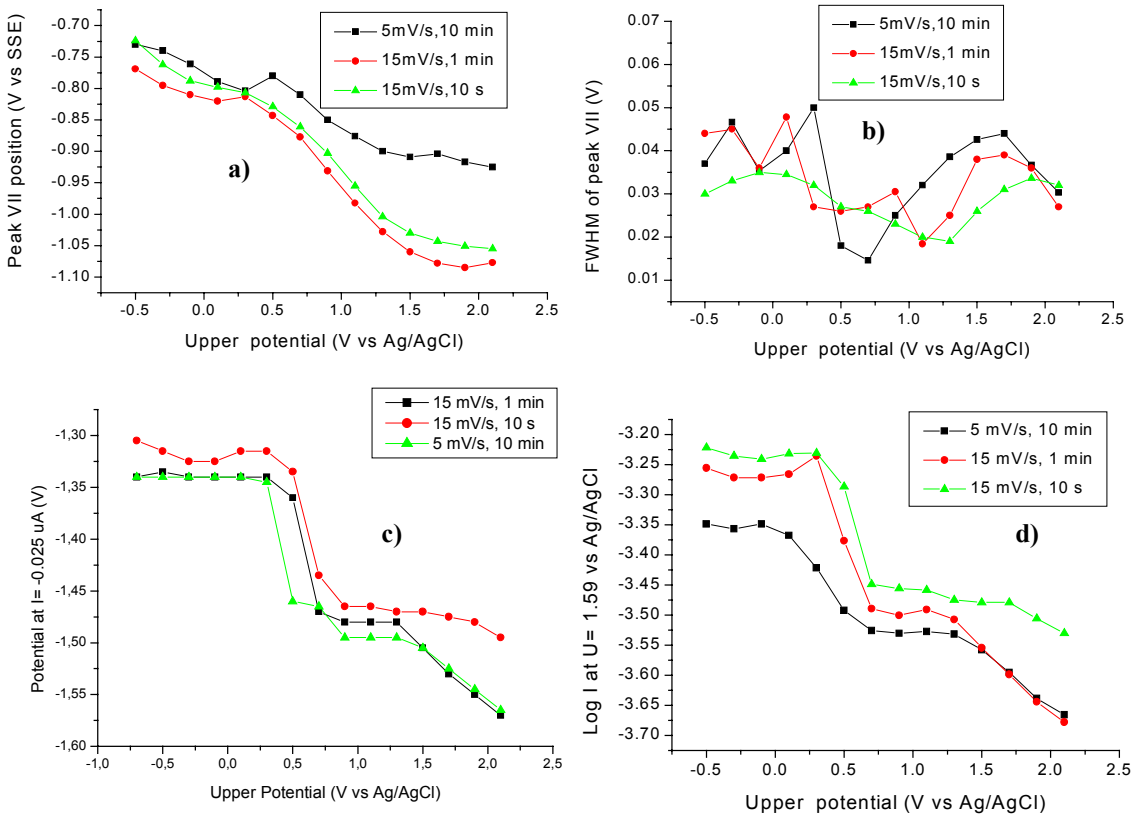

Fig. 5.8. *Analysis of the linear voltammetry results performed at different oxidation times and scan rates: a) Potential at which peak VII is present; b) Full Width at Half Maximum of peak VII; c) Potential values taken at I= -0.025 μA; d) Logarithm of the reduction intensity measured at –1.59 V. All the data are represented with respect to the upper potential applied. It can be observed that the shift of peak VII is approximately linear with respect to the upper oxidation potential, while for upper oxidation potentials beyond 0.5V vs Ag/AgCl the 'reduced layer' has a lower conductivity to the HER reaction (abrupt transition between 0.3-0.7V vs Ag/AgCl).*

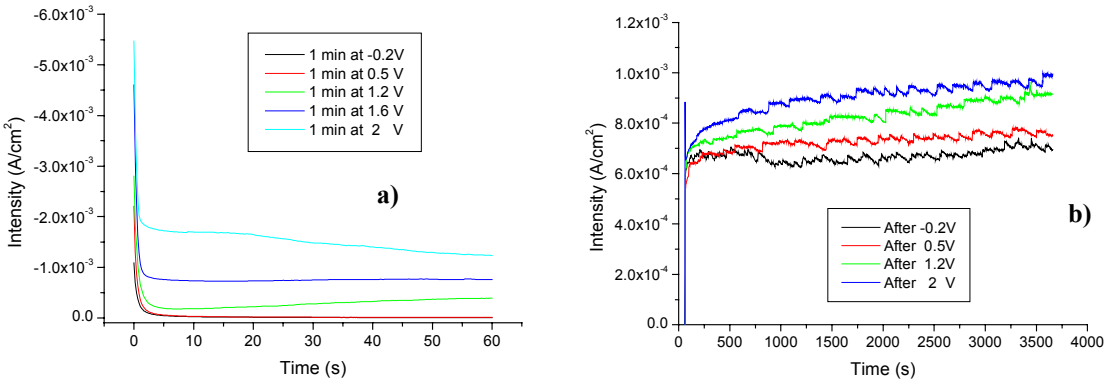

Fig. 5.9. *I-t curves of the same sample after successive oxidation-reduction processes: a) Transient curves when applying an oxidation potential; b) Transient curves observed at –1.6 V vs Ag/AgCl after the oxidation steps shown in a).*

Additionally, the effect of different oxidation and reduction times was studied. These results were presented in fig. 5.9. Thus, a fresh tin sample was firstly reduced at –1.6 V during 15 min (as usual) and then, oxidised at different anodic potentials and back to –1.6 V vs Ag/AgCl again. The results clearly show that the oxidation current is not yet stabilised after 1 min and that the roughness of the sample is progressively increased, as the reduction current increases with the successive steps. The noise observed in this last figure is due to the strong hydrogen bubbling present at this potential.

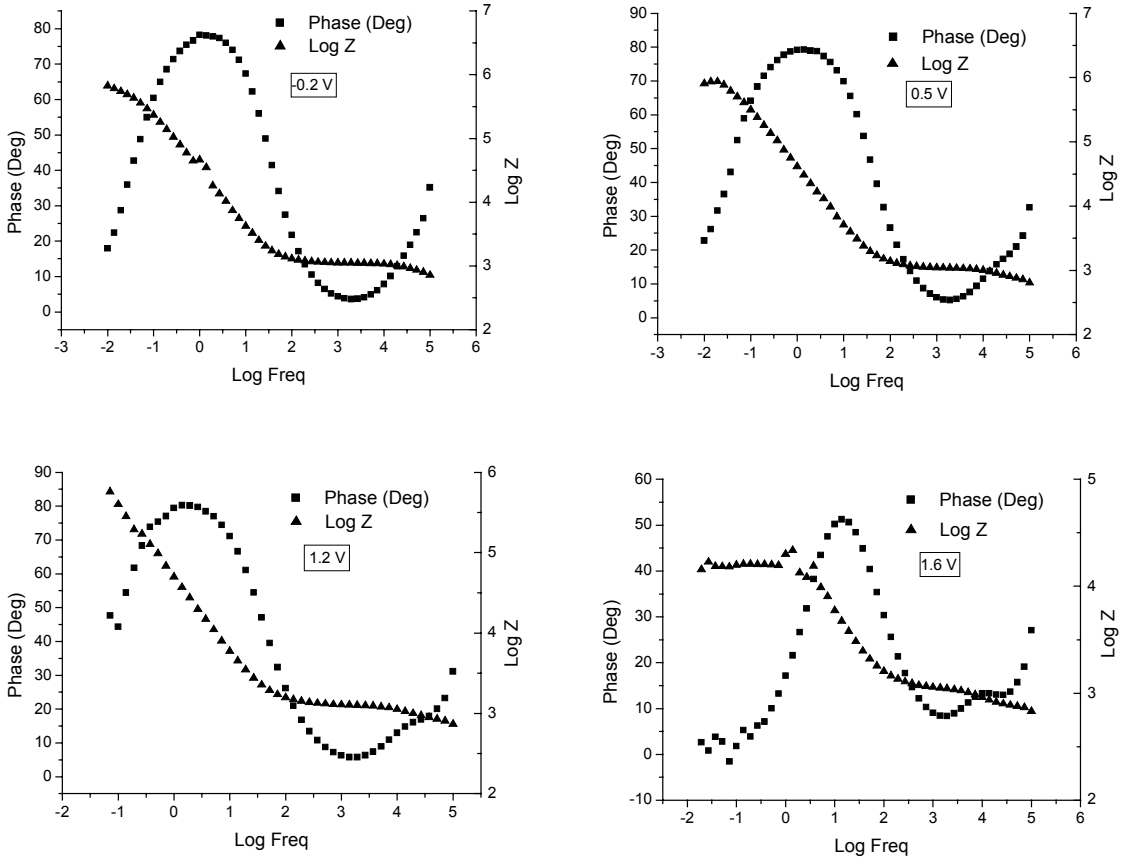

Fig. 5.10. *Bode plots obtained after 1 hour of oxidation at different potentials.*

To complete this study, several impedance measurements were made at different potentials. Thus, after 1 hour of oxidation at the desired potential (the time was chosen in order to be long enough to have a full oxidation process of the samples, i.e., the oxidation current density after this time were always very low (< 5 $\mu A/cm^2$)), the electrochemical impedance data were acquired. The results are summarised in fig. 5.10 and 5.11, that plot the Bode and Mott-Schottky graphs, respectively.

As it can be observed, different maximum in the Bode plots are observed when changing the potential.

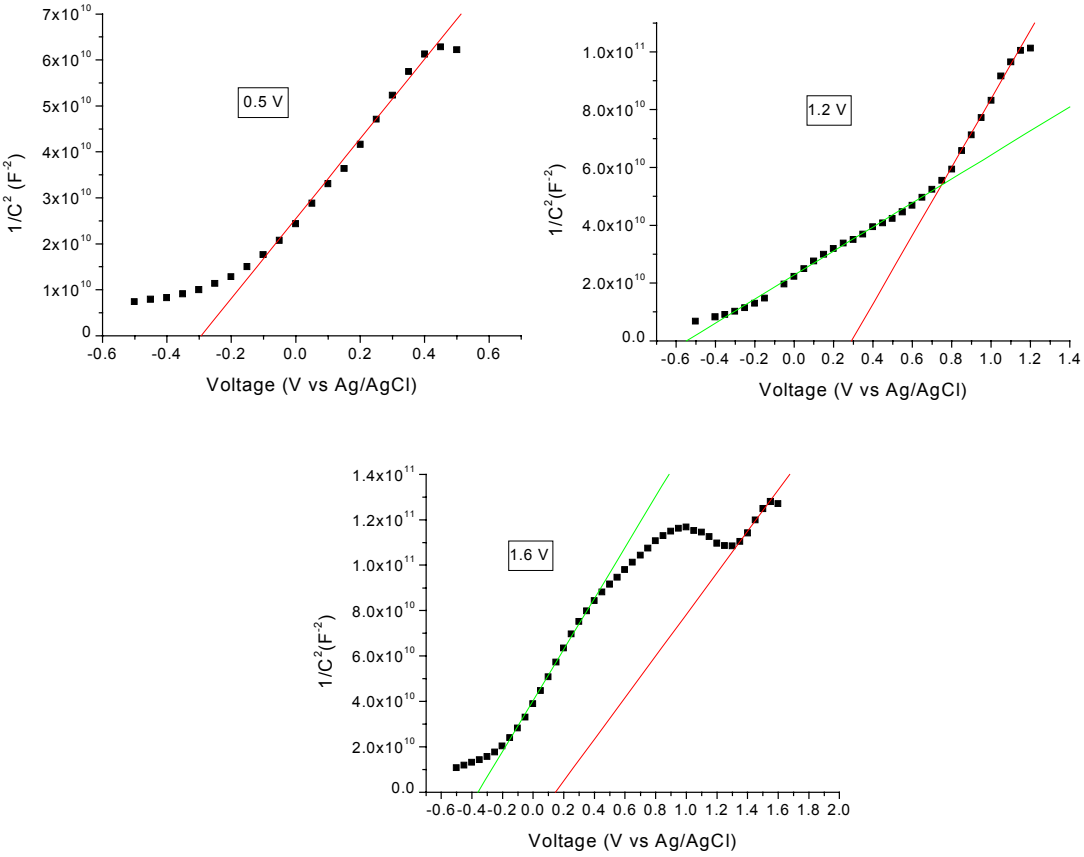

Fig. 5.11. *MS plots of samples oxidised at different potentials. The MS plots have been measured at the frequency of maximum phase of the corresponding Bode plot (fig. 5.10).*

	A	B	R	E_{FB} (V)
0.5 V	$2.6x10^{10}$	$8.7x10^{10}$	0.996	-0.29
1.2 V	$2.3x10^{10}$	$4.2x10^{10}$	0.991	-0.55
1.2 V	$-3.5x10^{10}$	$1.2x10^{11}$	0.997	0.29
1.6 V	$4x10^{10}$	$1.1x10^{11}$	0.998	-0.36
1.6 V	$-1.3x10^{10}$	$9.2x10^{10}$	0.996	0.15

Table 5.1. *Results of MS fitting (where y = a + bx).*

When fitting the Mott-Schottky, only the linear region was considered. The fitting results of the MS are summarised in table 5.1.

To complete the study presented below, there are two main aspects that would be of great interest to explore in order to have a deeper understanding of the oxidation behaviour of tin polycrystals: the discussion about the assignation of the observed peaks to Sn(II) or Sn(IV) species and the effect of the pH change. These two facts are closely related, as Sn(II) species have a low solubility at high pH (K_{ps} ($Sn(OH)_2$)= $5.45 \cdot 10^{-27}$) [215].

Thus, in order to obtain a concentration in solution of Sn(II) that can have observable effects in the voltammogram and avoiding the precipitation of $Sn(OH)_2$, the pH of the solution must be lowered. We have investigated the behaviour of tin in boric acid 0.15 M, that has pH=5.8. The voltammogram is shown in fig. 5.12, and it can be observed that the conductivity of the solution is very low, probably due to the formation of ionic pairs of boric acid. Thereby, to increase the conductivity, Na_2SO_4 0.1 M was added to the solution, obtaining the voltammogram showed in fig. 5.13. As it can be seen, there is a corrosion process of the sample in this solution. Fig. 5.14 shows together fig. 5.12, 5.13 and a voltammogram in borate buffer at pH=7.5. To know which was the origin of these corrosion processes, Na_2SO_4 0.1 M was added to the borate buffer at pH=7.5, and a similar voltammogram to that observed in fig. 5.13 was obtained. On the other hand, Na_3PO_4 0.1M was tested in the borate solution at pH= 7.5, and the voltammogram was similar to that discussed above (see, for example, fig.5.3.), with only a slight increase of the current of hydrogen evolution, thereby showing that the corrosion processes observed in fig. 5.13 are associated to reactions induced by the sulphate ions, and that in order to study tin in boric acid, Na_3PO_4 must be added. Nevertheless, it is also evident that the conductivity of the borate solution at pH=7.5 is high enough, as the presence of Na_3PO_4 does not alter the observed voltammograms. Thus, the presence of a supporting electrolyte is not necessary in this last case.

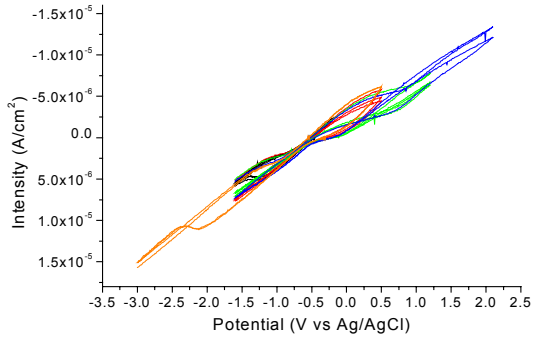

Fig. 5.12. *Voltammogram in H_3BO_3. Scan rate = 5mV/s.*

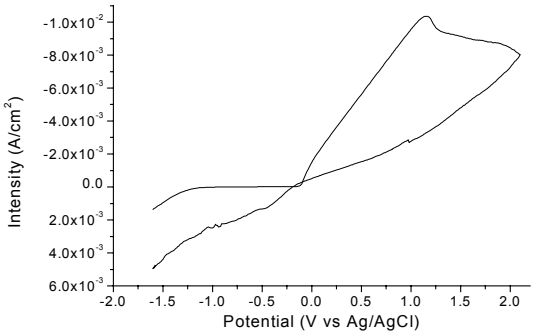

Fig. 5.13. *Same solution as in fig. 5.12, adding Na_2SO_4. Scan rate = 5mV/s.*

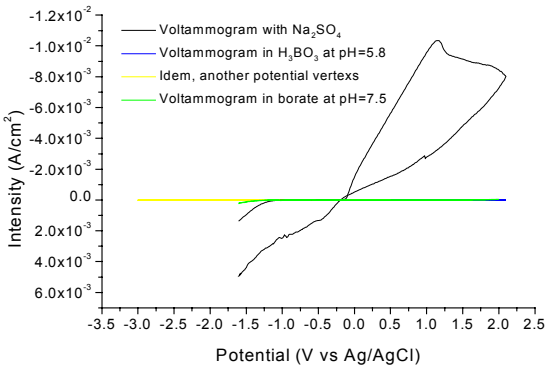

Fig. 5.14. *Comparison of tin voltammograms in different solutions. Scan rate = 5mV/s.*

5.2.2. Tin (100) single crystal

As it has been previously discussed, the study performed above has been made in order to provide us with a good knowledge of the oxidation/reduction behaviour of tin and tin oxides. In future work, this knowledge will be crucial to understand the gas sensing mechanism in tin oxides but, in order to study this kind of processes, the use of single crystals is preferred. The main reason is the fact that each crystalline face has a different behaviour with respect to a certain reaction, thereby making very complicate to extract conclusions from the features observed in polycrystals because in them the observed behaviour comes from a complex mixture of the behaviours of all the faces.

With respect to tin single crystals, no bibliography has been found concerning their use in electrochemical studies. Thereby, the first issue that must be accomplished in order to begin electrochemical studies with tin single crystals is the preparation of the surface. This process is extremely important, because for electrochemical studies it is necessary to have an initial reproducible surface with a low roughness and, in the case of single crystals, with preferred crystalline orientation.

In our case, we have studied tin (100) single-crystal. The as-received surface was quite rough, so it was necessary to make some process to polish it that also maintained the crystal orientation of the sample. This is not straightforward as, for example, mechanical polishing (described in the experimental section of this work, as it was the process used to prepare tin polycrystals) does not maintain the crystal orientation.

After some experimental work, we finally attained a good chemical polishing of the tin polycrystal surface, as can be observed both in fig. 5.15 (an interferometer image) and in figure 5.16 (a TMAFM image), by immersing it in a solution containing only HNO_3, CH_3COOH and glycerine.

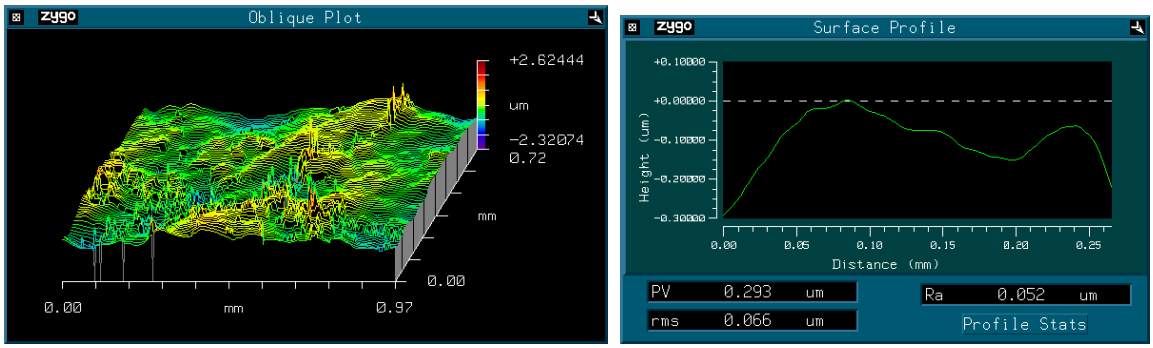

Fig. 5.15. *The figure on the left is an interferometric image of tin polycrystal surface after chemical polishing. Figure on the right gives the mean roughness (rms) of the surface.*

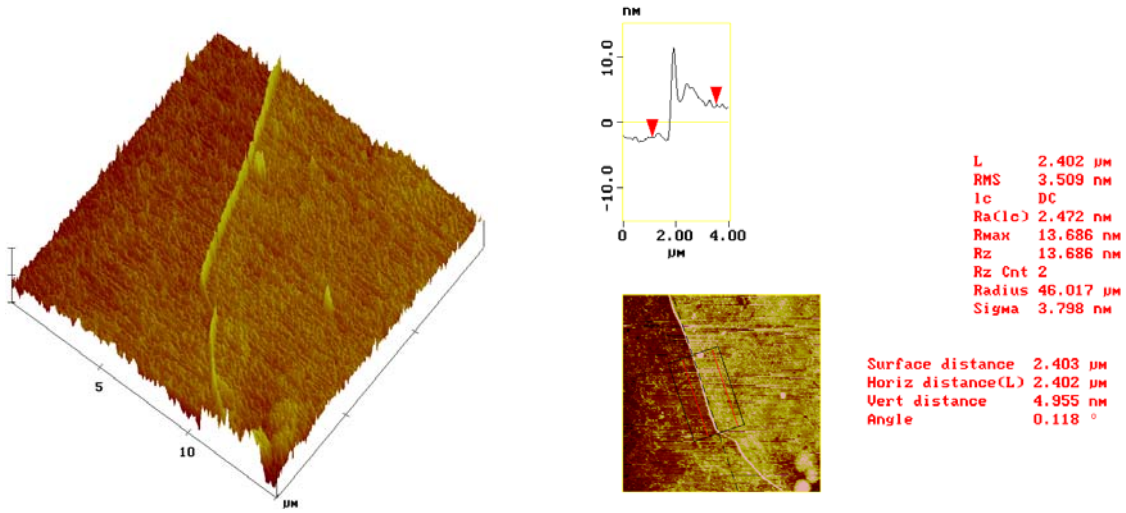

Fig. 5.16. *3D AFM image of polycrystal surface after chemical polishing. The image of the right side shows the mean roughness and the height of the steps found on the surface. Nevertheless, when the same solution was applied to the tin single-crystal surface, the resulting surface was unoriented, as showed in fig. 5.17.*

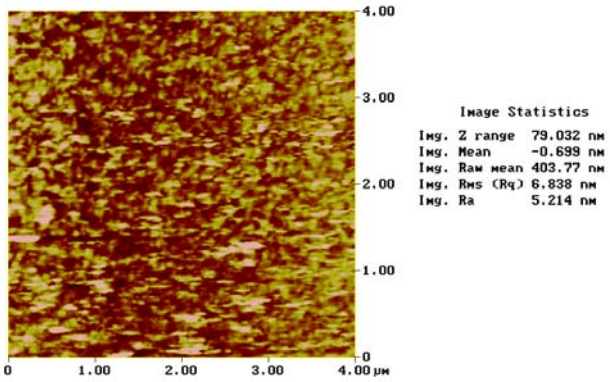

Fig. 5.17. *Contact AFM image of tin (100) single-crystal after chemical polishing with the same solution than the one used to polish tin polycrystals.*

As has been commented above, the preparation process must allow to have a preferred crystalline orientation. Thereby, this chemical polishing procedure was not enough and we finally applied another solution that contains only HCl and NH_4NO_3. After a few minutes in this solution, the surface of the tin single crystal (showed in fig. 4.18.) has a preferred crystalline orientation, as desired.

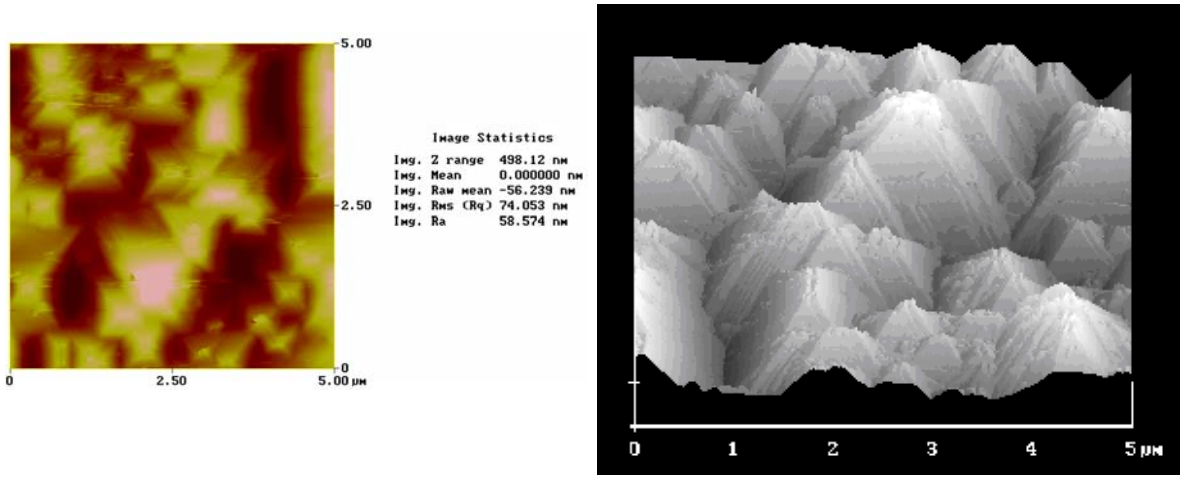

Fig. 5.18. *Roughness and 3-D AFM image of the tin single-crystal surface after chemical etching.*

The image showed in fig. 5.18. was reproducible all along the surface, and it has been tested many times. This surface is good enough to perform electrochemical studies. Nevertheless, as it can be observed, the roughness is quite high, making difficult to study processes by means of SPM techniques. Thereby, it was necessary to design another solution that allowed to maintain the preferred crystalline orientation and that reduced the mean roughness of the surface.

We were finally able to design suitable solutions to obtain a Sn (100) surface with preferred crystalline orientation and roughness low enough to allow SPM studies, as showed in fig. 5.19, just by using solutions containing only: HCl, NH_4NO_3 and glycerine. As it can be seen, the mean roughness of the surface is lower than that observed in fig. 5.18, thereby allowing SPM studies. This is also evident when seeing a detail of the faces of the pyramids of fig. 5.19, that is showed in fig. 5.20 together with a step that is found elsewhere throughout these faces.

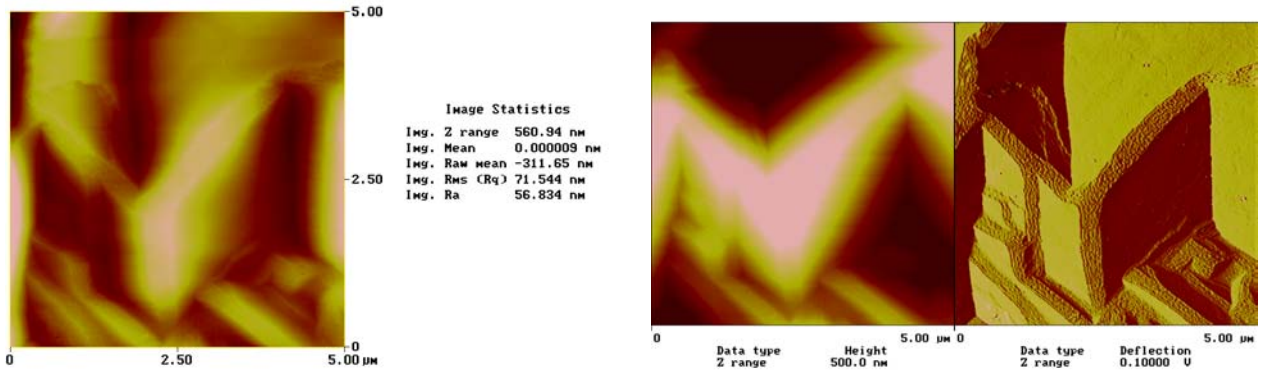

Fig. 5.19. *Contact AFM image of Sn (100) surface after treatment with the new solutions.*

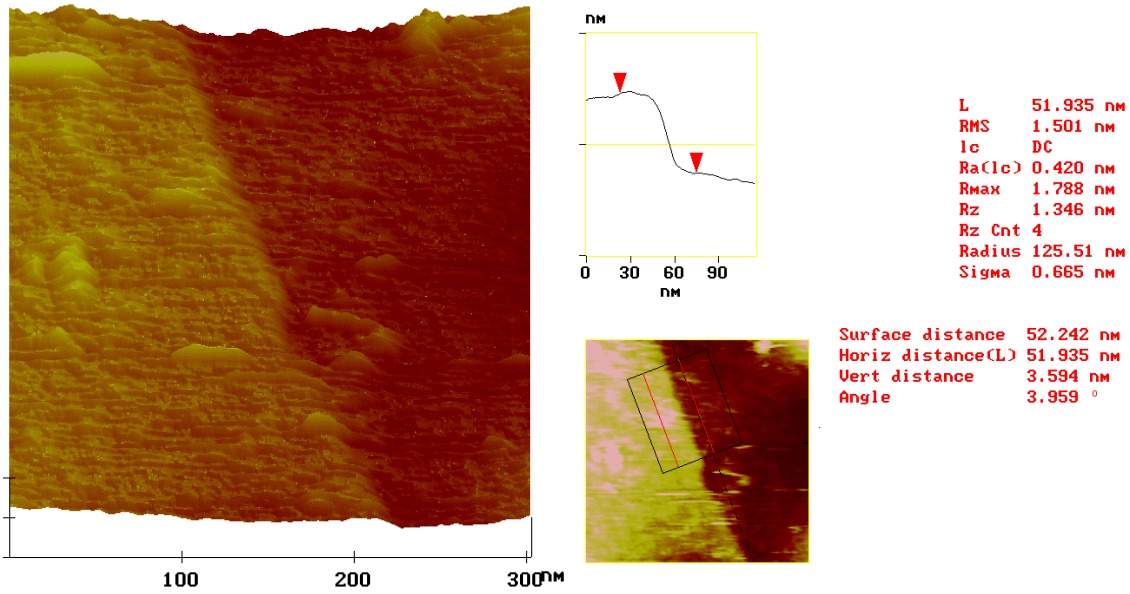

Fig. 5.20. *3-D AFM image of a face of a pyramid present on the surfaces treated with the final solution, together with the measure of one of the steps found throughout these surfaces.*

To allow a better understanding of the role of the different chemical agents present on the final solution, we will briefly show the surfaces of tin (100) single crystals obtained when substituting one of the chemical agents present in this solution. Thus, when substituting the nitrates by chlorides (changing NH_4NO_3 by NH_4Cl), no changes of the unetched surface were observed even after a long time, thus indicating that nitrates are the agents responsible for the preferred etching of the tin surface. Afterwards, when changing HCl by HNO_3, a precipitate (probably of tin hydroxide) was formed on the tin surface after some minutes of treatment. This is showed in fig. 5.21. Thus, the chlorides act as complexing agents of tin ions and are necessary to allow a full etching of tin, even though the pH of the solution is quite low.

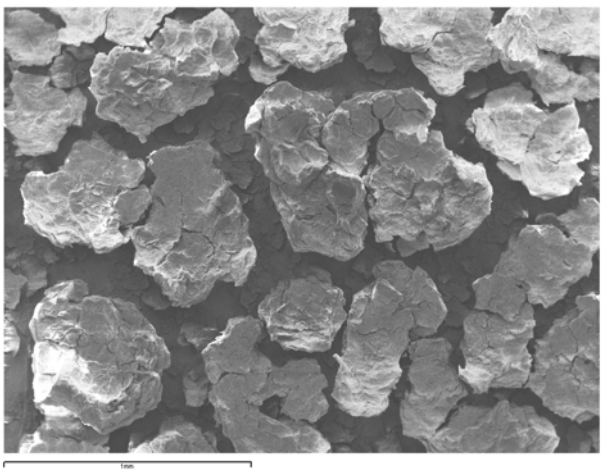

Fig. 5.21. *Tin (100) surface after etching without chlorides.*

Finally, as can be seen when comparing the composition of the solution used to obtain the surface showed in fig. 5.18 and the one used to obtain the surface showed in fig. 5.19, it is clear that glycerine is the responsible of the more "rounded" aspect of the last surface, also lowering the roughness.

It must be stated that, in order to obtain clean surfaces, a washing procedure must be performed to remove the impurities present, specially the glycerine. The procedure consists in: 1) Immersion of the sample in a hot trychloroethylene solution during 5 minutes; 2) Immersion in acetone during 5 minutes; 3, 4 and 5) Immersion in three different ethanol solutions for 5 minutes. Steps 2, 3, 4 and 5 were done in an ultrasonic stirrer.

Thus, we have developed a reproducible procedure to prepare Sn(100) surfaces either for electrochemical or SPM studies. Work is in progress to study different aspects of this system. To give a first insight of this system, we show the cyclic voltammogram, Bode and MS plots of Sn (100) single crystal in the same borate solution at pH=7.5 used for the polycrystal study. They are shown in fig. 5.22, 5.23, and 5.24, and MS fitting results are summarised in table 5.2.

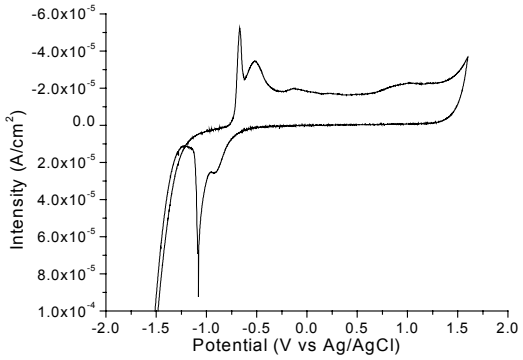

Fig. 5.22. *Cyclic voltammogram of Sn (100) in borate solution, pH= 7.5. Scan rate = 5mV/s.*

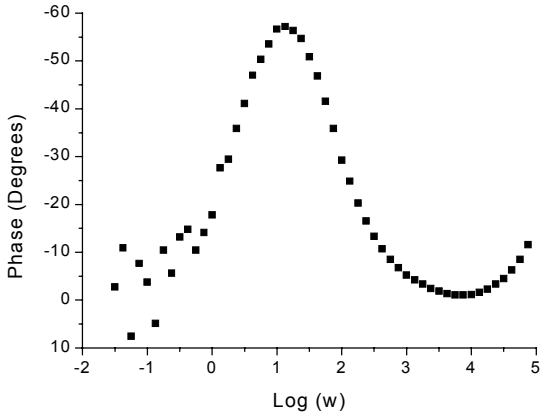

Fig. 5.23. *Bode plot of Sn (100) after oxidising for 2 hours at 1.6 V in borate solution, pH=7.5.*

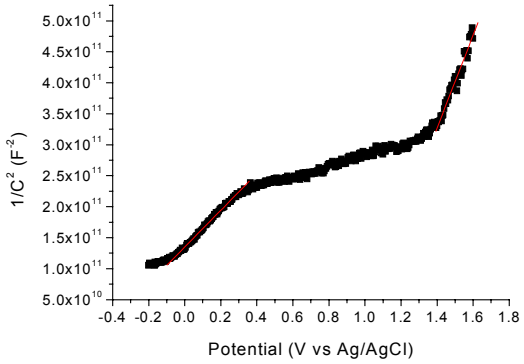

Fig. 5.24. *MS plot and fitting of Sn (100) after oxidising for 2 hours at 1.6 V in borate solution at pH= 7.5. It was measured at the frequency of maximum phase of the Bode plot (fig. 5.23).*

	a	b	R	E_{FB} (V)
1.6 V	-7.2×10^{11}	7.5×10^{11}	0.976	0.96
0.4 V	1.4×10^{11}	3×10^{11}	0.998	-0.46

Table 5.2. *Results of the fitting of MS plot of fig. 4.24. (y = a + bx)*

Together with these preliminary electrochemical results, in situ EC-STM studies of the oxidation of Sn (100) in borate buffer solutions are under development. The first results showed a surface where monoatomic steps are present, as can be seen in fig. 5.25. The mean height of the steps (3.12 Å) coincides with the c parameter of the unit cell of metallic Sn [216], thus indicating that the observed terraces correspond to the (001) planes of metallic tin.

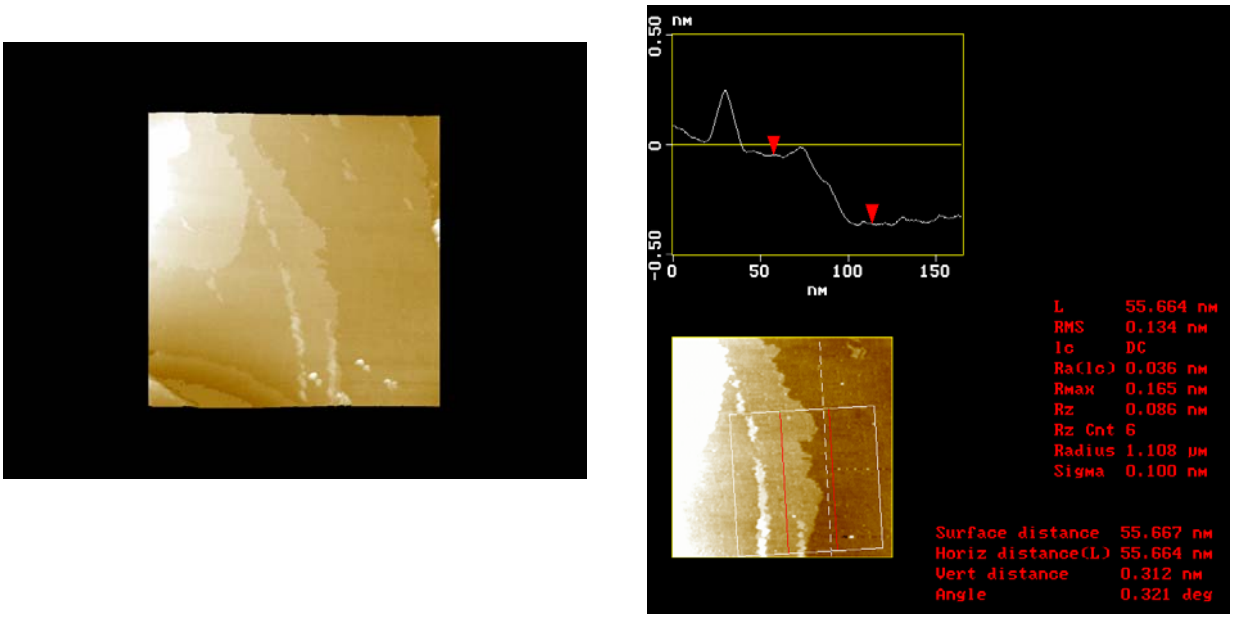

Fig. 5.25. *EC-STM image of Sn (110) in borate buffer solution at pH=7.5. Image taken after reduction of the sample at –1.6 V vs Ag/AgCl during 15 min and keeping the sample at -1.1V.*

Thus, as a first result, it has been observed that, when applying a potential scan at 5mV/s up to –0.2 V vs Ag/AgCl and scanning back to –1.1 V, i.e., when only peaks I, II and VII are present, the tin is dissolved and the oxide formed is precipitated, while after reduction similar steps as those showed in fig. 5.25 are observed. These results are summarised in fig. 5.26.

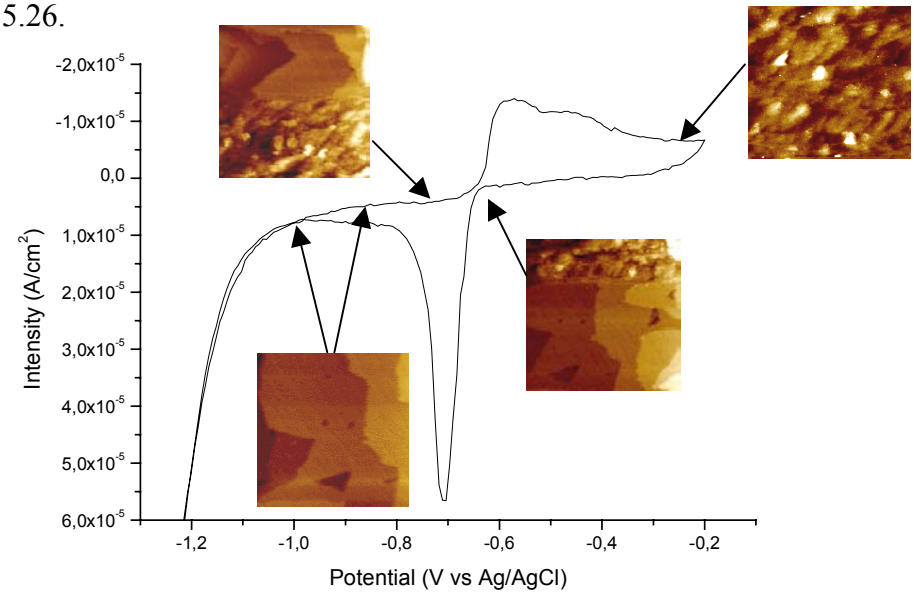

Fig. 5.26. *Complete cyclic voltammogram at 5 mV/s of Sn(100) in borate buffer solution at pH=7.5 together with the in-situ EC-STM images observed when scanning up to –0.2V.*

5.3. Discussion

With respect to the results presented in this section of the work, we will only discuss here the interpretation of the systematic study performed for tin polycrystals. As is discussed above, we have only begun the study of tin single-crystal that, at the present stage, has permitted us to obtain a surface suitable for electrochemical studies and new information about the redox processes at low upper potentials, but it was not the aim of this work to perform the systematic electrochemical study of tin single crystal. Nevertheless, this study will be performed in the future, and the results will be crucial for the understanding of the processes here discussed for tin polycrystals.

Thus, when looking at the results presented above for tin polycrystals throughout the literature [217-230] it can be said that, specially in 70's and 80's, a lot of studies have been done concerning tin electrochemical behaviour. With respect to studies similar to those here presented, the results can be summarised as follows:

- **Peak I:** This peak is attributed to the oxidation of metallic tin to $Sn(OH)_2$ or SnO. Recent studies in citric acid at pH= 6 [227-229] state that this process is diffusion-controlled, as the area of the peak is observed to increase adding Sn^{2+} or increasing the stirring rate.

- **Peak II:** It is attributed to the oxidation of the previously formed Sn(II), giving $Sn(OH)_4$. Some authors discuss the possibility of having a dissolution-precipitation mechanism.

- **Peak III:** This peak is only discussed once, in borate buffer at pH= 8.5 [220] and it is associated to the electrochemical dissolution of the formed oxide.

- **Peak IV:** In recent studies in citric acid [227-230], it has been attributed to a phase transition between the previously formed $Sn(OH)_4$ and SnO_2. The passivation region between this peak and the previous ones has been attributed to the progressive dehidratation of $Sn(OH)_4$ to SnO_2.

- **Peak V:** To our knowledge, no discussion of the oxygen evolution has been done. As stated, our experiments show that the current of oxygen evolution decreases with subsequent scannings, thereby saying that the passivation process alters both hydrogen and oxygen evolution.

- **Peak VI:** It has been associated with the apparition of SnO_2.

- **Peak VII:** In general, this peak is associated with the simultaneous reduction of the Sn(IV) and Sn(II) formed in peaks I and II to metallic tin. The shift of its position with respect to the anodic potential reached in the scan has also been previously observed.

- **Peak VIII:** No systematic study of the hydrogen evolution has been performed. Only in some studies in borate buffer at pH=8.4 it is said that hydrogen evolution diminishes very much when cyclic to anodic potentials more positive than 1.6 V vs SCE.

- **Peak IX:** No bibliography about this peak has been found.

In general, it is observed that the anodic charge is greater or equal to the cathodic one, and the difference between them increases with increasing the anodic potential applied. It has been also discussed the possibility, when arriving to high anodic potentials, of having an SnO_2 layer in contact with the metal and a layer of Sn(II) oxide or hydroxide in contact with the solvent. Several photoelectrochemical studies of this system have been performed and a photoelectrochemical response was obtained just after peak II, thereby attributing it only to Sn(IV) species.

When looking at the results presented above for tin polycrystals on borate buffer solution at pH=7.5, the peaks observed in the cyclic voltammograms can be assigned as follows:

- **Peak I and II:** These peaks correspond to the oxidation of metallic tin to Sn(II), probably forming tin(II) hydroxides The two peaks correspond to two different oxidation processes, occurring independently of the crystalline orientation, either in mechanically polished polycrystals or in chemically polished tin (100) single-crystal. It can be said that, as shown in fig. 5.26, in-situ EC-STM results show that the formed hydroxide is amorphous and that this first oxidation/reduction process (i.e., these two processes together with process of peak VII) is atomically reversible (undergoing a recrystallization process when reduction is applied) up to, at least, -0.2 V vs Ag/AgCl.

- **Peak VII:** As discussed above, this peak corresponds to the reduction of Sn(II) to metallic tin in an oxidation-reduction process that is completely reversible up to, at least, -0.2 V vs Ag/AgCl.

- **Peak III:** This peak probably corresponds to the dehydratation of the $Sn(OH)_2$ previously formed. Thus, the new VII peak that can be observed when oxidising at this potential (see fig. 5.5.) and that substitutes to the former VII peak corresponds to the reduction of SnO to metallic tin.

- **Between peaks III and IV:** At potentials between 0.5 and 0.9 V vs Ag/AgCl no peaks are observed in the cyclic voltammogram. Nevertheless, in fig. 5.8. it can be observed that peak VII shifts its position to more positive potentials, and the potential shift and hydrogen evolution also change. Probably, the possible formation of some SnO_x ($1<x<2$) (i.e., a change in the doping concentration of the oxide), would lead to the observed decrease of the hydrogen evolution and shift of the potential of peak VII (fig. 5.9).

- **Peak IV:** At the present state of the study, no clear assignation of this peak can be made, but it seems to be due to some kind of structural rearrangement.

- **Between peaks IV and V:** From 1.3 to 2.1 V vs Ag/AgCl, no further shift of peak VII is observed. Nevertheless, it is only in this potential interval where peak VI is present and, moreover, a further decrease of hydrogen evolution and change of the potential shift are observed. All these processes might indicate the thickness growth of the SnO_2 film, together with a change of its crystalline properties, that can be affected by the oxygen evolution.

- **Peak VI:** As it has been discussed above, this peak only appears when cycling until positive potentials greater than 1.3 V vs Ag/AgCl. Thereby, it is attributed to the reduction of SnO_2 to SnO.

- **Peak IX:** This peak is attributed to some fast surface reconstruction or recrystallization processes, as it is only observed when the scanning rate is fast enough.

Similar interpretations were previously reported in [217], where it was discussed that electrochemical oxidation of tin in borate buffer gives SnO up to +0.2V vs SSE and SnO is oxidised to SnO_2 between 0.2 and 1 V vs SSE. The high potential needed for the SnO_2 formation was then attributed to the fact that ionic conduction prevails to electronic one at low potentials. It is also discussed that the greater anodic charge value with respect to the cathodic one is due because half the anodic charge is used for the oxidation of tin and the other half dissolves metallic tin, forming stannites.

Most of the results presented so far can be accounted for by two different phenomena: the oxidation of the Sn electrode produces a layer whose semiconducting properties greatly influence its reducing behavior, as reported in tin and other metals, e.g. electrochemical properties of tin oxide [227-230] or iron oxide [231] and the formation of an oxide layer that hinders the HER, as the Sn electrode seems to have the highest HER capability where no oxide layer is present or when oxidizing at potentials lower than 0.5V vs Ag/AgCl (see fig. 4.8.c). Layers that have been formed at potentials higher than 0.5V vs Ag/AgCl display lower HER currents at a given potential, or require a higher potential ("HER overpotential") to yield the same HER current. Note that the "HER overpotential" is taken arbitrarily versus a reference at –1.59V vs Ag/AgCl.

Between peak II and 0.5 V vs Ag/AgCl, i.e. in the middle of the plateau, the HER overpotential remains unchanged, but the shift of peak VII (fig. 4.8.a) increases almost linearly. Since electrons for the reduction reaction must be supplied from the conduction band (CB) of the semiconductor, we attribute this shift to the shift of the CB edge. This could be a result of the progressive oxidation from Sn(II) to Sn(IV) that occurs in the plateau. The concentration of Sn(II) ("oxygen vacancies" which act as donor dopant atoms, see section 1.2 in page 6) is reduced, and results in two electronic effects:

- thickening of the space charge region (SCR) (see equation 2, page 8).
- separation between the CB edge energy and the Fermi energy:

$$U - U_c = (kT/e) \cdot \ln(N_c / N_d)$$

with U = electrode potential (Fermi energy), U_c = bandedge potential, N_c = effective density of CB states, N_d = doping density. Relation is valid if the semiconductor is far from degeneration and all donor impurities are ionized.

If this is the case, the experimental flatband potential (FB) should be independent of the potential of layer formation. Unfortunately, the Mott-Schottky plots employed to determine the FB are not very linear, especially for low anodic potentials, and this makes FB values very uncertain.

After 0.5V vs Ag/AgCl, there is a sudden increase in HER overpotential (-150mV) that we attribute to the existence (persistence) of an oxide layer that hinders the HER and is not immediately reduced at –1.6V vs Ag/AgCl.

Beyond 0.5V vs Ag/AgCl, peak VII overpotential also increases and with a higher rate that at lower oxidating potentials. This can be due to further reduction of N_d, which thickens the SCR and separates the CB from the Fermi level. The same situation continues up to 1.5V vs Ag/AgCl and does not seem to be affected by peak IV. Thus it seems that peak IV is related to structural rearrangements not having a noticeable effect on either of these processes. Indeed, in borate buffer the apparition of peak IV coincides approximately with that of peak VI, being their shape more characteristic of a layer transformation than of a well-defined redox process in the electrolyte. We attribute peak VI to the reduction of dehydrated SnO_2 to SnO. In citric acid, peak IV has been attributed to a phase transition between $Sn(OH)_4$ and SnO_2 [227-230].

The onset of the oxygen evolution reaction (OER) at 1.5V vs Ag/AgCl coincides with a plateau in the peak VII overpotential, and a further increase in the HER overpotential (-100mV). Within our proposed interpretation, we suggest that the CB edge cannot shift any further because layer doping (Sn(II) content) has decreased to a saturation level. The shift in HER overpotential may now be due to further increase of hindering of HER by the oxide layer formed, probably because of the increase of the thickness of this layer. It is worth mentioning here that subsequent scans result in a reduction of the OER current. In fact, EC-STM experiments confirm that, when applying an oxidation potential high enough, no atomic reversibility of the oxidation-reduction process is observed on Sn(100) monocrystals even after reducing them during 15 minutes at –1.6VvsAg/AgCl.

Obviously, the experimental results presented in the previous section support the proposed model and succession of events, but do not constitute a proof for it. Further verifications

are required, and in that sense two lines of experiments are under course: Raman spectroscopy of the layer under potentiostatic control, and electrochemical STM imaging and spectroscopy of Sn(100) monocrystals. From the latter, we expect to confirm the values of CB edge potential by direct electron injection from the STM tip into the CB of SnO_2 following a method recently developed in our laboratory [232]. With respect to Raman, it is being performed because of its ability to distinguish different compounds and between Sn(II) and Sn(IV) and preliminary in-situ Raman experiments under potentiostatic control in borate have shown that the oxide formed between 0.3 and 0.9V vs Ag/AgCl (i.e., in the plateau after peak III) is different from the one formed after peak II. In fact, the oxide formed after peak III is semiconducting and shows luminiscence both under red and under green laser light. This luminiscence changes with respect to the anodic potential applied and also with respect to the time of oxidation, thereby supporting the previous discussion, where the oxides formed in this region were attributed to a progressive oxidation of Sn(II) to Sn(IV), with a subsequent change of doping concentration. Moreover, the SnO_2 A_{1g} Raman band is observed only after oxidizing at potentials higher than where peak IV is present and this band does not disappear even after reducing at -1.6V vs Ag/AgCl during 15 minutes, thereby giving support to the formation of oxides that cannot be fully reduced and that hinder the HER.